

## MODELED MESOSCALE GRAVITY WAVES: CONTINUOUS SPECTRUM AND ENERGY CASCADE

Chungu Lu<sup>1†</sup>, Steven Koch, Fuqing Zhang, and Ning Wang

*NOAA Research-Forecast Systems Laboratory, Boulder, Colorado*

<sup>†</sup> *[In collaboration with the Cooperative Institute for Research in the Atmosphere, Colorado State University]*

### 1. Introduction

Several of our previous theoretical and observational studies have pointed to the linkage of gravity waves and turbulence in the atmosphere (Koch et al. 2005; Lu et al. 2005a, 2005b). Gravity waves interacting with turbulence are in scales right above the turbulent inertial range, with the wavelength typically on the orders from a few to a few tens of kilometers. However, gravity waves (with pressure perturbation of a few millibars) have shown their strong presence in mesoscales, typically on the order of a few hundred kilometers. One obvious explanation for this scale separation of gravity waves is that different-scale waves are generated by different sources or a source with different intrinsic scales. Apart from this mechanism, there is also a possibility that these waves with different scales are genotypically related, i.e., smaller-scale gravity waves are generated from larger-scale gravity waves via wave-wave interactions.

Using spectral analysis and wavelet transformation technique, we analyzed modeled gravity waves from an idealized model simulation. The

computed spectral power density from modeled vertical velocity field presents a continuous expansion of wave scales from low wavenumbers to high wavenumbers with time. Wavelet analysis actually localized these waves in physical space. A time series of these wavelet-decomposed waves tends to indicate that smaller-scale waves are spawned by larger-scale waves.

### 2. Modeled mesoscale gravity waves

Zhang (2004) has studied the gravity-wave generation associated with an upper-level jet streak using the NCAR/Penn State mesoscale model (MM5, Dudhia 1993). The model simulation was composed of an outer domain and two nested domains with 90, 30, and 10-km horizontal grid spacing, respectively. In this study, we will concentrate on the most inner domain with the finest horizontal resolution. This inner domain simulation is initialized at 72 hours after the time integration of the outer domain begins, and the model runs to 120 h, when a set of gravity waves are fully developed. Figure 1 shows the gravity wave generation in the vicinity of an upper-level jet streak. The shaded region indicates the location of an upper-level jet with wind in excess of  $40 \text{ m s}^{-1}$  (denoted as vectors in the graph), the thick-blue curves denote pressure fields,

---

<sup>1</sup> Corresponding author address: Dr. Chungu Lu, NOAA/FSL; e-mail: Chungu.Lu@noaa.gov.

and the thin-red contours are horizontal divergence, which present evident wave structure.

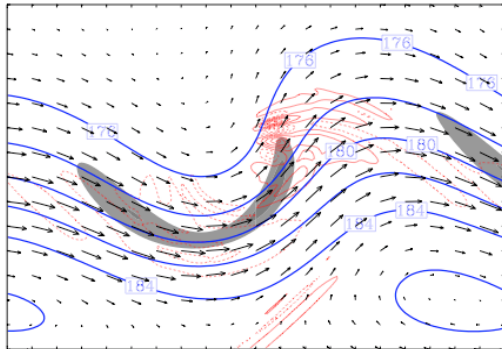


**Fig. 1:** Gravity waves associated with an upper-level jet system (shaded region). The thick-blue curves are pressure field, the thin-red curves are divergence field, and winds are depicted in the sized vectors. The distance between tick marks is 300 km.

Figure 2a and 2b are horizontal views of the vertical velocity field (thin-black contours) and potential temperature (thick-blue contours) at 13-km altitude. At 108 h (Fig. 2a), a loosely defined wave with a broad scale of 500-600 km in wavelength was present. At 120 h (Fig. 2b), this wave was fully developed and had tightened its scale to about 150 km in wavelength. The red lines in these two figures indicate the vertical cross-sections that we are taking for further analysis. Figure 3a and 3b show the vertical velocity field (thin-blue curves) and potential temperature (thick-red curves) viewed in these vertical cross-sections at 108h and 120h, respectively. One can see that some internal gravity-wave signals occurred initially, and then these waves extended downward vertically. Again, the waves clearly showed scale contraction with time.

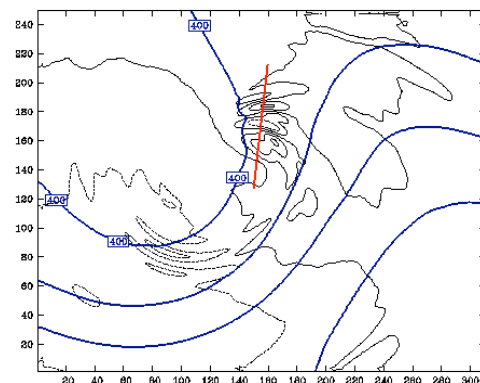
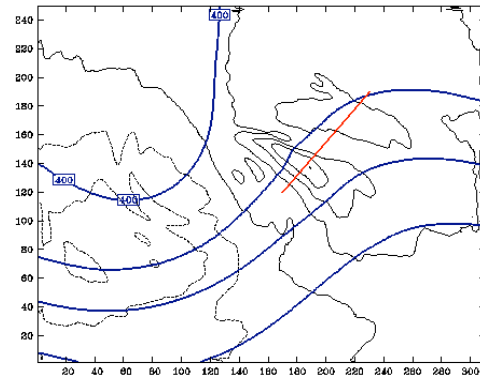


**Fig. 2:** Vertical velocity (thin-black contours) and potential temperature (thick-blue curves) at a) 108h, and b) 120h. The red lines indicate the vertical cross-section analyses conducted in Fig. 3. The horizontal scale in the graph is 200 km between tick marks.

### 3. Spectral analysis

Because spectral analysis contains exact information about wave scales, we first conduct scale decompositions of the vertical velocity field at the 13-km level for the hourly output from 108 h to 120 h from the MM5 model simulation, using 2D spectral transformations. Figure 4a to 4e are the corresponding Fourier power spectral density of vertical velocity, plotted as functions of horizontal wavenumbers,  $n_x$  and  $n_y$ .

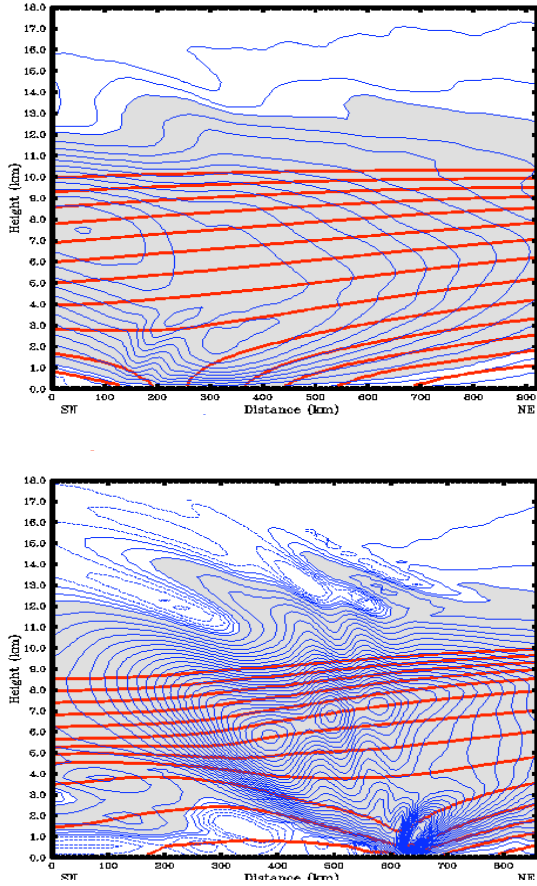
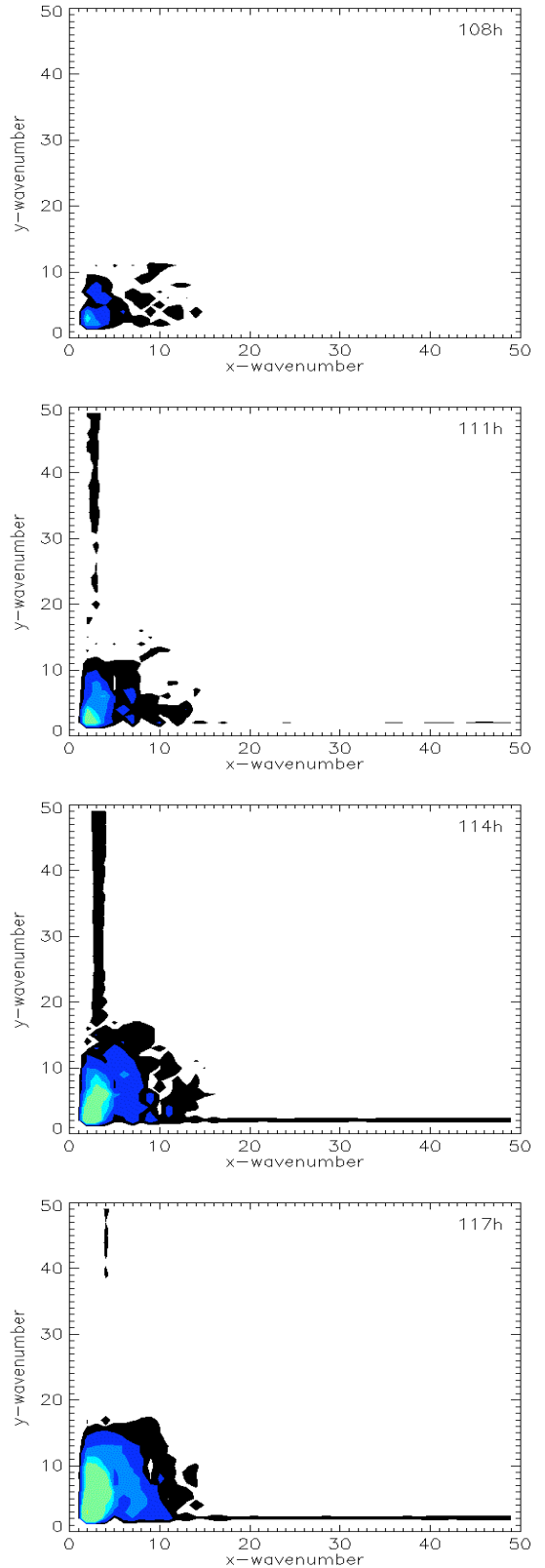


**Fig. 3:** Vertical cross-section view of vertical velocity (thin-blue curves) and potential temperature (thick-red curves) at a) 108h, and b) 120h.

One can see that at 108h (Fig. 4a), most wave energy resides in the low wavenumbers. As time increases, wave energy begins to spread to higher and higher wavenumbers. In particular, at 120h (Fig. 4e), relatively high wavenumbers, such as  $n_x = n_y \sim O(10)$  have already possessed substantial wave energy.

We can further quantify this continuous expansion of the wave spectrum and energy cascade process by defining a total wave number:  $n = \sqrt{n_x^2 + n_y^2}$ . With this total wavenumber, we can calculate

the power spectral density of gravity waves in a



time-spectrum space, shown in Fig. 5. The original data is truncated with a size

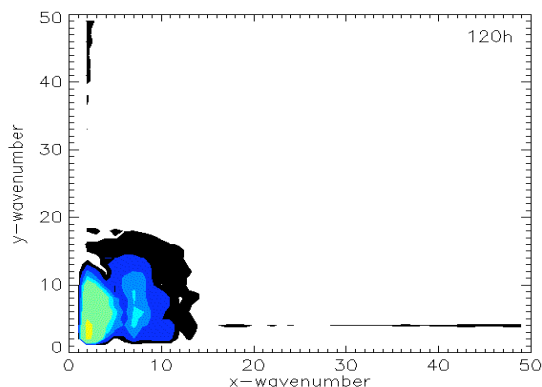


**Fig. 4:** 2D Fourier spectra of vertical velocity at a) 108h, b) 111h, c) 114h, d) 117h, and e) 120h.

of  $128 \times 128$ , so that the wavelength can be calculated approximately by  $\lambda = 128 \times \sqrt{2} \times 10 \text{ km} / n$ . At 108h, the wave energy is concentrated at approximately 600-km wavelength. At subsequent times from 111 to 120 hours, the wave energy continuously feeds into higher wavenumbers, while maintaining the same energy level at the initial low wavenumbers. The later notion—no dissipation of energy at low-wavenumber—may be an artifact of a current numerical model, in which turbulence dissipation and high-wavenumber waves’ consumption on the energy level of the low-wavenumber waves and mean flows have not been parameterized effectively and correctly.

#### 4. Wavelet-based Hovmöller diagram analysis

The above spectral analysis provided useful information about the wave scales, but could not actually realize these waves in the physical space. A two-dimensional wavelet transformation can localize a 2D physical field,  $f(x, y)$ , in space, as well as characterize its

scales (Wang and Lu, 2005). Mathematically, this transformation can be expressed as

$$\hat{f}[s, (x, y)] = \iint f(x', y') \psi_{s, (x, y)}^*(x', y') dx' dy'$$

where

$\psi_{a, (x, y)}(\zeta, \xi) = |a|^{-1} \psi[a^{-1}(\zeta - x, \xi - y)]$  is a locally-supported transformation kernel (asterisk denotes the complex conjugate). The scale parameter  $a$ , which is inversely proportional to the wavelength, and the parameter  $(x, y)$ , which gives a horizontal spatial location, are respectively the dilation and translation parameters. In this study, we use the Halo mother function as the transformation kernel.

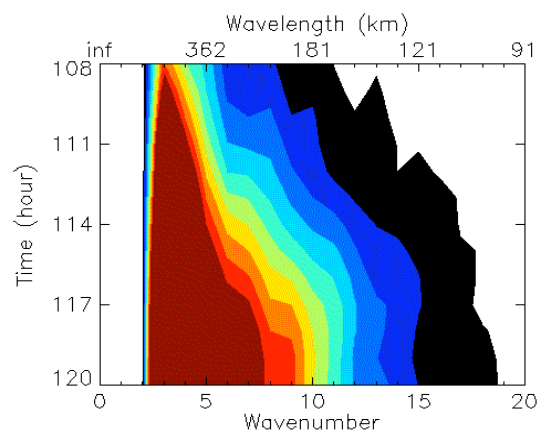


**Fig. 5:** Time-wavenumber analysis of modeled gravity waves.

By combining the scale information provided by the spectral decomposition and wavelet transformation, we can now construct a wavelet-based Hovmöller diagram by ordering the wavelet-transformed vertical velocity field according to its time sequence. Figure 6 displays this wavelet-based Hovmöller diagram. The images are the wavelet-decomposed power spectra, while the white contours are the original vertical

velocity field. The diagram shows the steepening of these gravity waves with time, going from 108h, at the bottom panel, to 120h, towards the top panel, as they propagate to the north-east direction initially and to the due north direction at later times.

On the other hand, the wavelet decomposition at later times should also present a continuous spectrum of low-wavenumber waves, which we have chosen not to include here. However, the persistence of these low-wavenumber waves at all times poses real perplexity of its physical understanding. The under-resolvable processes in the current numerical (finite-dimensional) models may have been treated incorrectly, as we discussed in the previous section.

## 5. Summary and conclusions

In this study, we analyzed the spectrum of the modeled gravity waves and localized these waves in physical space using a wavelet decomposition technique. The spectral analysis suggested an energy cascade mechanism for the generation of small-scale gravity waves from their large-scale counterparts. This mechanism is consistent with the theory of steepening of gravity waves via wave-wave interaction, discussed by Weinstock (1986). This may provide a link between wave-turbulence interaction (on the spatial scales of kilometers and sub-kilometer) and mesoscale gravity waves (on a spatial scale of several hundred kilometers) associated with an upper-level jet system (on a spatial scale of thousand kilometers). On the other hand, the continuous expansion of the

energy power spectrum indicated a continuous energy input into the whole spectrum of the modeled gravity waves. This may suggest that current numerical models may be at fault in dealing with the dissipation effect of small-scale features, and therefore, may need more studies on this problem.

*Acknowledgments.* The authors are grateful to Dr. John Brown for the NOAA internal review, and to Susan Carsten for technical editing. This research is in response to requirements and funding by the U. S. Federal Aviation Administration (FAA). The views expressed are those of the authors and do not necessarily represent the official policy or position of the FAA.

## References

- Dudhia, J., 1993: A nonhydrostatic version of the Penn State/NCAR mesoscale model: Validation tests and simulation of an Atlantic cyclone and cold front. *Mon. Wea. Rev.*, **121**, 1493–1513.
- Koch, S. E., B. D. Jamison, C. Lu, T. L. Smith, E. I. Tollerud, C. Girz, N. Wang, T. P. Lane, M. A. Shapiro, D. D. Parrish, and O. R. Cooper, 2005: Turbulence and gravity waves within an upper-level front, in press, *J. Atmos. Sci.*
- Lu, C., S. Koch, and N. Wang, 2005a: Stokes parameter analysis of a packet of turbulence-generating gravity waves. In press, *J. Geophys. Res.*
- Lu, C., S. E. Koch, B. D. Jamison, and E. I. Tollerud, 2005b: Spectral and structure function analysis of upper-troposphere horizontal velocity fields. Part I: Interaction of turbulence and gravity waves, Kelvin-Helmholtz instability, and wave breaking. Submitted to *J. Geophys. Res.*
- Zhang, F., 2004: Generation of mesoscale gravity waves in upper-tropospheric jet-front systems. *J. Atmos. Sci.*, **61**, 440–457.
- Wang, N., and C. Lu, 2005: A two-dimensional continuous wavelet algorithm and its application to meteorological data analysis. Submitted to *J. Atmos. Oceanic Technol.*
- Weinstock, J., 1986: Finite amplitude gravity waves: Harmonics, advective steepening, and saturation. *J. Atmos. Sci.*, **43**, 688–704.

**Fig. 6:** Wavelet-based Hovmöller diagram. The images are power spectra of wavelet transformed vertical velocity, and the white contours are the original vertical velocity. Each panel constitutes a skewed horizontal-spatial domain of 1800x1500 km. The stacks of the panels are ordered according to time (hourly) from 108h at the bottom to 120h at the top.

